DE GRUYTER OPEN

Analele Universităţii de Vest din Timişoara
Vol. LVII, 2013
Seria Fizică

DOI: 10.1515/awutp -2015-0110

THE AHARONOV-BOHM EFFECT AND TRANSPORT PROPERTIES IN GRAPHENE NANOSTRUCTURES

Mihai Lungu*, Raluca Giugiulan, Antoanetta Lungu, Madalin Bunoiu and Adrian Neculae

West University of Timisoara, Faculty of Physics, Bd. V. Parvan, no.4, 300223 Timisoara, Romania

E-mail: lmihai@physics.uvt.ro

Article Info
Received: 22.03.2013
Accepted: 05.04.2013

Keywords: Flue gas filtration, Nanoparticle separation, Dielectrophoresis, Recovery, Purity, Separation efficiency

Abstract

This paper investigates the possibility to improve the filtering process of flue gas by separation of suspended nanoparticle using dielectrophoresis. The study focuses on the particles having an average radius of about 50–150 nm, that cannot be filtrated by classical techniques but have a harmful effect for environment and human health. The size distribution nanoparticles collected from the flue gas filters of a hazardous waste incinerator plant were evaluated. Based on obtained experimental data and a proposed mathematical model, the concentration distribution of nanoparticle suspended in flue gas inside a microfluidic separation device was analyzed by numerical simulations, using the finite element method. The performances of the device were described in terms of three new specific quantities related to the separation process, namely *Recovery*, *Purity* and *Separation Efficiency*. The simulations could provide the optimal values of control parameters for separation process, and aim to be a useful tool in designing microfluidic devices for separating nanoparticle from combustion gases.

1. Introduction

Filtration of nanoparticle suspended in flue gas is an important technological challenge, as in urban environment the burning processes including waste incinerators or diesel emissions are responsible for the emission of a significant amount of nanoparticle [1]. The presence in the environment of nanoparticle with size ranging from 50nm to 150 nm has a profound impact on human health. Once inhaled, due to their tendency to remain trapped in the inner respiratory ways, infiltrate into the blood and cannot be eliminated, because the macrophage cells cannot identify them. From a public health standpoint, the size of a particle is as important as its composition, recent research showing that although raw materials may not be dangerous, they can become toxic under the form of nanoparticle [2,3]. Although the nanoparticles have smaller masses than microparticles, their number is at least four orders of

magnitude higher than the number of all other particles found in the flue gas. Sources of polluting emissions are generally equipped with various filters that capture the micron particles, but permit nanoparticle to escape in atmosphere [4,5].

The most promising technique for nanoparticle trapping and controlled spatial separation is a method based on dielectrophoresis (DEP), phenomenon in which a spatially non-uniform AC or DC electric field induces a dipole moment in a dielectric particle. Hence, the particle undergoes a DEP motion under the resulting translational force. This force does not require electrically charged particles; the strength of the force depends on the medium and particle's electrical properties, particle's shape and size, and on the applied electric field amplitude and frequency [6,7]. Having the ability to manipulate particles based solely on their dielectric properties and size [8,9].

This paper presents an assessment regarding the entrapment of nanoparticle dispersed in flue gas using dielectrophoresis. The first part of the study deals with the experimental evaluation of two relevant ash samples collected from the flue gas filters of a hazardous waste incinerator plant and reveal the presence of nanoparticle. In the second part, the study exploits numerical simulations concerning the behavior of nanoparticle with size ranging from 50 to 150 nm in a microfluidic channel. The concentration profile of nanoparticle suspension inside a microfluidic separation device is calculated and the performance of the device is analyzed in terms of three new specific parameters of separation process, called *Recovery, Purity* and *Separation Efficiency*. This study aims to identify a suitable way to predict accurately the particle entrapment by using numerical solutions of the DEP-flow equations for the fluid and find the optimal values of the control parameters for separation process, useful in designing of microfluidic devices for separating nanoparticle from combustion gases.

2. Material and methods

Materials employed for this study were two probes, named as A and B, consisting in samples of ash resulted from the combustion of different wastes, collected monthly from filters of Pro Air Clean Timisoara hazardous waste incinerator, within a period of two months.

For dimensional characterization, we prepared for each of the three probes a mixture of 5 mg ash in 100 ml distilled water at room temperature, and put it to rest for 20 minutes, in order to decant the microparticles. Then we collected the remained slurry liquid and analyzed the particle size/concentration distribution using a Nano Sight LM 10 nanoparticle visualization system, using nanoparticle-tracking analysis method. Figure 1 illustrates the size/concentration distribution of particles for probe A (figure 1a) and probe B (figure 1b),

after a decantation time of 20 minutes. The distribution diagrams indicate four significant groups of nanoparticle, with sizes of 44 nm, 67 nm, 109 nm, and 180 nm in probe A, and four significant groups of nanoparticle, having sizes of 55 nm, 100 nm, 155 nm, and 275 nm in probe B.

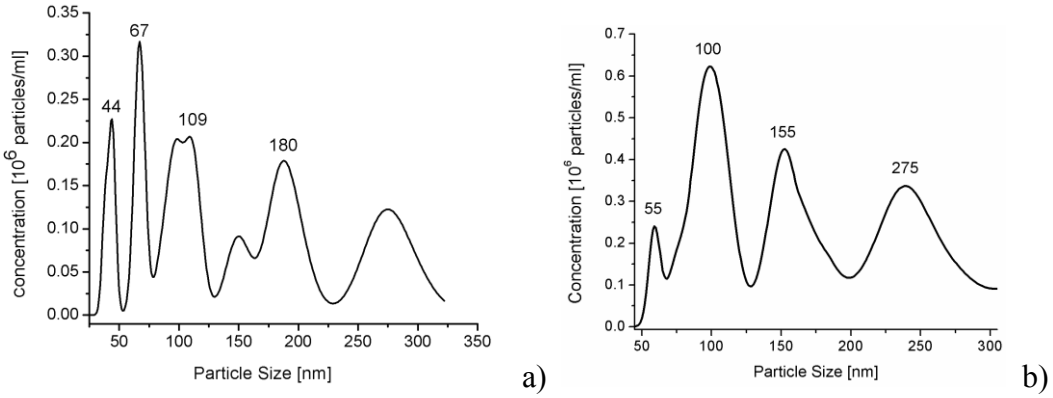

Figure 1: The size/concentration distribution of nanoparticle for probes A and B, obtained with the visualization system of nanoparticle, Nano Sight LM10, after 20 minutes of decantation time.

These analyses show that the gas resulting from the combustion of waste contains nanoparticle. They are, however, relevant to our study because the results suggest the existence of a much larger quantity of nanoparticle in the combustion waste gases than originally detected. In the following, our study will focus mainly on the particles with radii smaller than 200nm, potentially harmful for human health.

3. Theory

The time averaged dielectrophoretic (DEP) force acting on a spherical particle situated in an AC electric field can be written as [6,8,9]:

$$\left\langle \mathbf{F}_{DEP} \right\rangle = 2\pi a^3 \varepsilon_m \,\mathrm{Re}\left[\tilde{K}(\omega)\right] \nabla\left(\left|\nabla V_R\right|^2 + \left|\nabla V_I\right|^2\right), \qquad (1)$$

where a is the particle radius, ω the angular field frequency and $\mathrm{Re}[\tilde{\cdot}]$ indicates the real part of a complex phasor $\tilde{\cdot}$. V_R and V_I are the real and imaginary part of the electric potential phasor, $\tilde{V} = V_R + jV_I$. For a homogeneous medium, the electric potential satisfy the Laplace equation $\nabla^2 \tilde{V} = 0$. The quantity $\tilde{K}(\omega) = (\tilde{\varepsilon}_p - \tilde{\varepsilon}_m)/(\tilde{\varepsilon}_p + 2\tilde{\varepsilon}_m)$, named the complex Clausius–Mossotti (CM) factor, is a measure of the effective polarizability of the particle, where $\tilde{\varepsilon}_p$ and $\tilde{\varepsilon}_m$ are the complex dielectric permittivities of particle and medium. The CM factor depends on the dielectric properties of the particle and medium, and on the frequency of the applied electric field [7]. The variation in the real part of this factor results in a frequency-dependent dielectrophoretic force that is unique for a particular type of particle.

When $\mathrm{Re}\left[\tilde{K}(\omega)\right] > 0$, the particle is attracted to the locations of maximum electric field intensity and repelled from the minimum, known as positive dielectrophoresis (pDEP). When $\mathrm{Re}\left[\tilde{K}(\omega)\right] < 0$, situation refers to as negative dielectrophoresis (nDEP).

The macroscopic behavior of a suspension of spherical particles of radius a in a fluid of viscosity η is modeled by considering the mechanical equilibrium between an external force (DEP force in this case) and the Stokes drag force. For computational efficiency, a non-dimensional method is employed: the electric potential was scaled with the amplitude of the applied signal, V_0, the distances were scaled with the electrode width d, while for the time, velocity and particle volume fraction we used the scales of d^2/D, D/d, and φ_0 (the initial average volume fraction), where D is the diffusion coefficient of the particles. In terms of dimensionless quantities (denoted by prime symbol), the DEP force (1) becomes:

$$\left\langle \mathbf{F}_{DEP} \right\rangle = F_{0DEP} \nabla' \left(\left| \nabla' V_R' \right|^2 + \left| \nabla' V_I' \right|^2 \right), \tag{2}$$

where $F_{0DEP} = 2\pi a^3 \varepsilon_m \mathrm{Re}\left[\tilde{K}(\omega)\right] V_0^2 / d^3 \right)$ is a quantity that measures the intensity of the external field. The dynamics of the system of nanoparticle in flue gas is governed by the transport equations [7,10]:

$$\mathbf{v}' = \mathbf{u}' + Q\mathbf{F}', \ \nabla \mathbf{u}' = 0, \tag{3a}$$

$$\frac{\partial \varphi'}{\partial t'} + \nabla \cdot \mathbf{j}' = 0, \text{ where } \mathbf{j}' = \varphi' \mathbf{v}' - \nabla \varphi', \tag{3b}$$

where $\mathbf{u}'$ and $\mathbf{v}'$ are the fluid and particle velocities, $Q = 2a^2 F_{0DEP} d / 9\eta D$ is a characteristic force constant, proportional to the external field intensity, $\mathbf{F}'$ is related to the dielectrophoretic external field as will show further, t' is the time, $\mathbf{j}'$ is the particle flux, and φ' is the particle volume fraction.

4. Results and discussion

After the dimensional analysis of the probes, we move on to setting prerequisites for building of a realistic DEP device for nanoparticle trapping from flue gas. Based on the results obtained in the previous section our numerical study deals with the computation of the concentration field for the nanoparticle suspension inside a microfluidic separation device, considering only the positive component pDEP of the dielectrophoretic force. We analyzed the numerical results in terms of three new parameters called *Recovery*, *Purity* and *Separation Efficiency,* correlated with the concentration field. This approach offers a more

suggestive characterization of the capabilities of the device regarding the separation process of nanoparticle from flue gas. All the numerical simulations were performed using a partial differential equations solver, FreeFEM++, based on the finite element method [5,7]. For the computation of the pDEP force, we first solved the Laplace equation for the real and imaginary components of the electric potential, together with the associated boundary conditions. The computational domain and the boundary conditions can be assumed as shown in figure 2, in which the particular case $d=l=30\ \mu m$ and $H=2d=60\ \mu m$ was considered. We neglected the electrodes height, according to a previous analyzes presented in [7]. Similar boundary conditions hold true for the imaginary part of the electric potential phasor. Details about the validation procedure of the program and an analysis of the dielectrophoretic force distribution are given in [7].

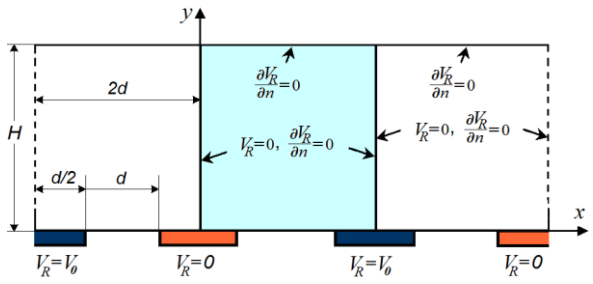

Figure 2: The geometry of the computational domain and the boundary conditions for the real part V_R of the electric potential phasor.

The schematic representations of a typical microfluidic DEP separation device with an interdigitated electrode array, revealing its main geometric parameters, and the simplified geometry used in computations are given in figure 3. The device has a rectangular cross section $\left(L_x = L, L_y = 2H\right)$ with two rows of electrodes placed on both the bottom and top surfaces as illustrated in the left hand side of the figure. Due to the symmetry of the device and considering the electrodes much longer than their width, the problem can be treated in two dimensions. Taking into account the periodic distribution of the electrodes and magnitude of the dimensionless DEP force, for the calculation of concentration field, we consider further a simplified computational domain, with neglecting the height of electrodes and the flow field described by a classical Poiseuille profile (the right hand side of the figure 3):

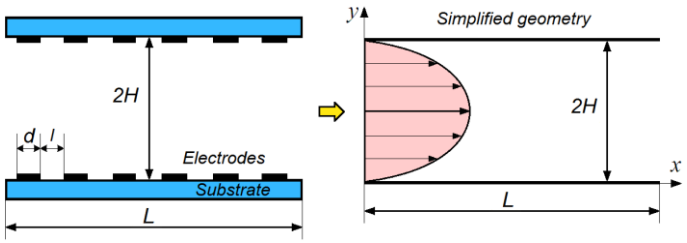

Figure 3: Schematic representation of a dielectrophoretic chamber used for DEP separation (left), and the simplified geometry used as computational domain for the computation of the concentration field (right).

Considering the length L of the device large in comparison with the electrodes width d, and assuming a harmonic potential $\tilde{V}$ $_0$ exp$(i\omega t - qx)$ imposed at the boundaries of the separation device, by solving the Laplace equation $\Delta\tilde{V}$ $=$ the analytical solution for the electric potential is:

$$\tilde{V}(x,y) = V_0 \exp(-iqx)\cosh qy / \cosh qd \,. \tag{5}$$

V_0 is the amplitude of the applied electric potential, $q = 2\pi/\lambda$ the wave number and λ the wavelength of the traveling wave. In this case, the DEP force becomes [7]:

$$\mathbf{F}_{DEP} = F_{0DEP}\mathbf{F}' \,. \tag{6}$$

where $\mathbf{F}' = \left(K'\cosh by, \sinh by, 0\right)$ corresponds to the term $\mathbf{F}'$ in (3a), K' is the ratio of the real and imaginary parts of the Clausius-Mossotti factor, and $b = 2qd$ is the dimensionless wave number. For further calculations, we will consider the analytical form of DEP force given in (6). To simulate the behavior of a suspension subjected to dielectrophoretic force, equations (3a)-(3b), with the expression for DEP force (6), were solved for various values of the parameter Q, corresponding to different intensities of the dielectrophoretic force. This parameter describes the global influence of several physical quantities on the manipulation process: it strongly depends on the applied voltage, carrier fluid and particle physical properties as permittivity and dimension. Thus, Q varies according to a square law with the applied voltage, and according to a cubic law with respect to particle dimension. Taking into account the influence of the velocity field on the concentration profile analyzed in [12], we considered a typical value of 10 μm/s for the maximum flow velocity in all the computations. To obtain a reference value for Q in a typical microfluidic device for DEP manipulation of particles with radius a=100 nm in air, we considered for the real part of the CM factor the value Re$\left[\tilde{K}\right]$ [11], $V_0 = 10$ V for the amplitude of the electric potential and

$\lambda = 120\mu m$ for the wavelength of the traveling wave. The computations of the concentration distribution inside the device were performed for values of the parameter Q ranging from 0.5 to 10. The concentration field calculated in the simplified computational domain for the reference value $Q = 1$ (a=100 nm, Re[illegible], $V_0 = 10$ V, $\lambda = 120\mu m$), where particles are attracted to the electrodes due to the pDEP effect, is shown in figure 4 a). Due to the symmetry of the problem, the nanoparticle distribution does not depend on the horizontal coordinate. For further analyses, we delimited a zone of interest having height *H*, measured from the bottom to the middle of the device, and an arbitrary width.

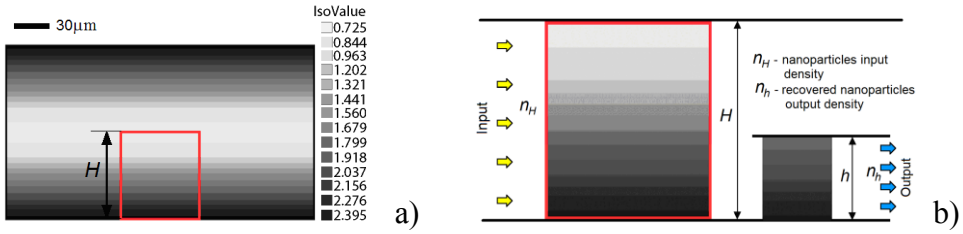

Figure 4: The calculated concentration field for $Q = 1$. The zone of interest marked by a rectangle of height *H* and arbitrary width (a). Close-up on the input zone (left) – with the zone of interest delimited from the middle to the bottom of the device (height *H* and arbitrary width) marked in red, and the output zone (right), considered as the recovery area, placed close to the electrodes and extending a distance *h* into the fluid (b).

The numerical simulation indicates that the concentration field presents a layered structure, which allows an analytical description as a function of a single spatial variable, *C(y)*, depending on the vertical coordinate *y*. Since the particle density is highest in the regions surrounding the electrodes, we considered the recovery area placed close to the electrodes and extending a distance *h* into the fluid, as in figure 4 b).

To obtain an efficient separation one must collect as many particles from the fluid suspension as possible, but at high values of particle concentration. In order to do this, a compromise value for the output width *h* ($0 \le h \le H$), is desirable: for a smaller *h* one separates a more concentrated fluid, while for a larger *h* one collects more particles.

For the quantitative analysis of the separation process, we define the following set of parameters, related to the particles concentration distribution *C(y)*:

- The recovered mass at the output, named as product or *Recovery* (*R*), representing the performance or effectiveness of the separation, related to particles found in the output:

$$R = \int_0^h C(y)dy\,. \tag{7}$$

- The recovered nanoparticle output density, defined as a function of concentration at output:

$$n_h = (1/h)\int_0^h C(y)dy\,. \tag{8}$$

- The *Purity* (*P*) of the product, that means quality of the separated fraction (i.e. the fraction of the separated nanoparticle concentration in the output), defined as:

$$P = \frac{n_h - n_0}{n_{\max} - n_0}, \tag{9}$$

where $n_0 = 1$ is the value of the particle density in the absence of the dielectrophoretic force and $n_{\max}$ is the particle density for $h \to 0$.

- The *Separation Efficiency* (*SE*) that provides more flexibility to evidence the efficiency at a certain stage of the separation, defined as:

$$SE = R + P - 1\,. \tag{10}$$

Next, we discuss the significance and the behavior of these parameters in relation to the proposed model. Figure 5 shows a typical distribution of the concentration field for different output widths *h* and DEP force intensities Q.

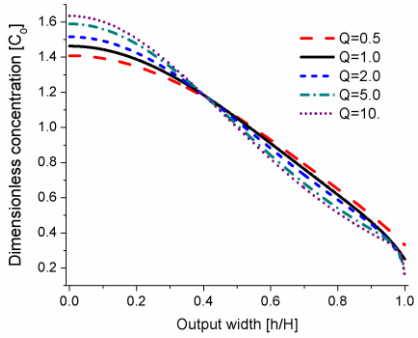

Figure 5: Distribution of the nanoparticle concentration in the recovery zone for different output widths *h* and DEP force intensities Q.

For all DEP force intensities the calculated concentration field reaches a maximum value at *h*=0 (near the electrodes) and a minimum value at *h*=*H* (in the central plane of the device). As expected, the maximum value of the concentration field increases with the intensity of the DEP force. Figure 6 shows the calculated values of *Recovery*, *Purity* and *Separation Efficiency* versus at various output widths *h* for a separation device having electrodes of $d = l = 30\mu\text{m}$, and an applied voltage of $V_0 = 10$ V on the electrodes. The computations were performed for three different values of particle radius, *a*=50nm, 100nm and 150 nm, values

corresponding to the ones revealed in the particle size/concentration distribution diagram presented in figures 1.

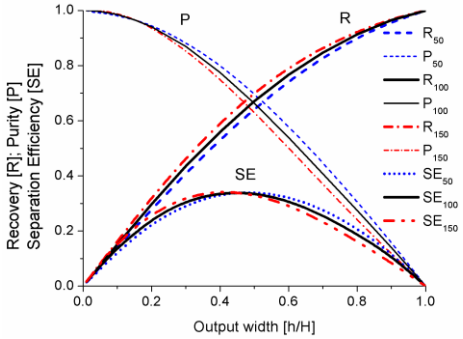

Figure 6: *Recovery*, *Purity* and *Separation Efficiency* versus the ratio *h/H*, calculated for three different values of particle radius: *a*=50nm, 100nm and 150 nm. The subscripts in the legend denote the corresponding values of particle radius.

One observes that *Separation Efficiency* first increases when increasing the output width *h*, achieves a maximum approximately at the intersection of *Recovery – Purity* plots, then decreases with *h*. One notices a quite low influence of the particle size on the separation efficiency. With increasing *h,* the amount of particles remained in the output (recovered mass) increases too, while *Purity* decreases. *P=1* corresponds to the maximum value of the particle concentration in the product, while *R=1* corresponds to the case when all the material ends up in the product. Therefore, a compromise must be found between the purity of the product, which will set the amount of the product. A reasonable choice for this compromise value is the maximum of *SE* curve. According to the presented separation diagram, the maximum separation accuracy is obtained at intermediate values of the ratio *h/H*, between the maximum leftmost and rightmost values of *SE*, corresponding to *a*=50nm and *a*=150nm.

5. Conclusions

This paper presents a set of experimental and numerical results regarding the filtering process by the entrapment of nanoparticle from flue gas using dielectrophoresis. The experimental results show that the analyzed ashes contain nanoparticle, the study focusing on the particles with radii smaller than 200nm, potentially harmful for human health. The numerical results for the distribution of the pDEP force inside a typical DEP device, and the concentration distribution profile of nanoparticle suspended in a flue gas under DEP influence show that, for particular values of the applied voltage at the command electrodes, nanoparticle in suspension tend to concentrate onto the channel walls, function of their sizes. The quantities *Recovery*, *Purity* and *Separation Efficiency* delineate a global image of the influence of the simulation parameters in the separation process. The analysis performed in

the frame of the presented mathematical model and geometry allows us to predict the value for the output width *h* to optimize the separation process. These simulations can help to find the appropriated geometric parameters of the microfluidic separation device, leading to the enhancing of the performance of filtering process.

Acknowledgments

This work was supported by a grant of the Romanian National Authority for Scientific Research, CNCS – UEFISCDI, project number PN-II-ID-PCE-2011-3-0762.

References

[1] F. Sbrizzaia, P. Faraldib, A. Soldatia, *Chem. Eng. Sci.* **60** (2005) 6551.

[2] D. Rickerby, M. Morrison, *Report from the workshop on nanotechnologies for environmental remediation*, JRC Ispra. (2007).

[3] P. Minutolo, L. Sgro, M. Costagliola, M. Prati, M. Sirignano, A. D'Anna, *Chem. Eng. Trans.* **22** (2010) 239.

[4] M. Chang, C. Huang, *J. of Environ. Eng.* **127** (2001) 78.

[5] M. Lungu, A. Neculae, M. Bunoiu, *J. of Optoelectronics and Advanced Materials* **12** (2010) 2423.

[6] R. Pethig, *Biomicrofluidics* **4** (2010) 022811.

[7] A. Neculae, C. Biris, M. Bunoiu, M. Lungu, *J. Nano. Res.* **14** (2012) 1.

[8] N. G. Green, A. Ramos, H. Morgan, *J. Elstat.* **56** (2002) 235.

[9] C. Barbaros, L. Dongqing, *Electrophoresis* **32** (2011) 2410.

[10] S. Shklyaev, A. Straube, New J. Phys. **10** (2008) 1.

[11] I. Malaescu, R. Giugiulan, M. Lungu, N. Strambeanu, *Romanian Journal of Physics* **59** (2014) 7.

[12] A. Neculae, R. Giugiulan, M. Bunoiu, M Lungu, *Rom. Rep. Phys.* **66** (2014) 3.